

Rapidity dependence of global polarization in heavy ion collisions

Zuo-Tang Liang,^{1,*} Jun Song,^{2,†} Isaac Upsal,^{1,3,‡} Qun Wang,^{4,§} and Zhang-Bu Xu^{1,3,¶}

¹*Institute of Frontier and Interdisciplinary Science,
Key Laboratory of Particle Physics and Particle Irradiation (MOE),
Shandong University, Qingdao, Shandong 266237, China*

²*Department of Physics, Jining University, Jining, Shandong 273155, China*

³*Physics Department, Brookhaven National Laboratory, Upton, New York 11973, USA*

⁴*Department of Modern Physics, University of Science and Technology of China, Hefei, Anhui 230026, China*

We use a geometric model for the hadron polarization with an emphasis on the rapidity dependence. It is based on the model of Brodsky, Gunion, and Kuhn and that of the Bjorken scaling. We make predictions for the rapidity dependence of the hadron polarization in the collision energy range 7.7-200 GeV by taking a few assumed forms of the parameters. The predictions can be tested by future experiments.

I. INTRODUCTION

In non-central collisions of heavy ions at high energies a huge orbital angular momentum (OAM) is generated. Through spin-orbit couplings in parton-parton scatterings, hadrons can be globally polarized along the OAM of two colliding nuclei [1–3]. In a hydrodynamic picture, the huge OAM is distributed into a fluid of quarks and gluons in the form of local vorticity [4–9], which leads to the local polarization of hadrons along the vorticity direction [10, 11] (for a recent review of the subject, see, e.g., [12]).

The global polarization of Λ and $\bar{\Lambda}$ has been measured in the STAR experiment in Au+Au collisions in the collision energy range 7.7-200 GeV [13, 14] through their weak decays into pions and protons. The magnitude of the global polarization is about a few percent and decreases with increasing collision energies. Hydrodynamic and transport models have been proposed to describe the polarization data for Λ and $\bar{\Lambda}$ from which the vorticity fields can be determined [8, 9, 15–21]. Then, through an integration of the vorticity over the freezeout hyper-surface [10, 11], the global polarization of Λ and $\bar{\Lambda}$ is obtained and agrees with the data [20–24].

The previous STAR measurement of the global polarization is limited to the central rapidity region. How the polarization behaves in the forward rapidity region can shed light on the polarization mechanism. The STAR collaboration are currently working on a series of upgrades in the forward region, which will add calorimetry and charged-particle tracking in the rapidity range [2.5, 4], and are expected to collect the data of Au+Au collisions at 200 GeV in 2023. Then Λ and $\bar{\Lambda}$ may be constructed in this forward region, allowing for the measurement of their polarization.

In this paper, we will give a geometric model for the hadron polarization with an emphasis on the rapidity dependence. This work is the natural extension of a previous work by some of us [25]. The geometric model is based on the model of Brodsky, Gunion, and Kuhn (BGK) [26] and that of the Bjorken scaling [25]. The BGK model can give a good description of the hadron's rapidity distribution in nucleus-nucleus collisions.

The paper is organized as follows. In Sect. II, we give formulas for the average longitudinal momentum and local orbital angular momentum using the method of Ref. [25] where the rapidity distribution of hadrons is given by the BGK model. In Sect. III, we use the hard sphere and Woods-Saxon model for the nuclear density distribution to calculate the rapidity distribution of hadrons. In Sect. IV, the hadron polarization from the local orbital angular momentum is calculated with the WS nuclear density distribution. By constraining the parameter by the polarization data at mid-rapidity, we make predictions of the polarization in the forward rapidity region. The summary is given in the last section.

*Electronic address: liang@sdu.edu.cn

†Electronic address: junsong2006@163.com

‡Electronic address: iupsalp@gmail.com

§Electronic address: qunwang@ustc.edu.cn

¶Electronic address: xzb@bnl.gov

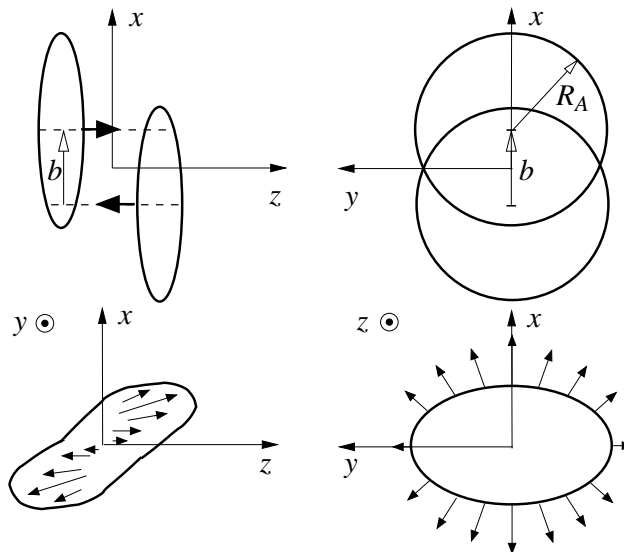


Figure 1: The schematic figure taken from [25] for non-central heavy ion collisions with impact parameter \mathbf{b} pointing to x direction. The orbital angular momentum is in $-y$ direction.

II. AVERAGE LONGITUDINAL MOMENTUM AND LOCAL ORBITAL ANGULAR MOMENTUM

There is an intrinsic rotation of the initially produced matter in the reaction plane in non-central heavy ion collisions. The rotation can be characterized by tilted local rapidity distribution of produced hadrons toward the projectile and target direction in the transverse plane. We consider non-central collisions of two nuclei $A + A$: the first one is regarded as the projectile moving in z direction while the second is regarded as the target moving in $-z$ direction, see Fig. 1 for illustration. The impact parameter is in the direction from the target to the projectile, i.e. in x direction. The orbital angular momentum (OAM) is in the direction that is determined by the vector product of the impact parameter and the projectile momentum, $\mathbf{b} \times \mathbf{p}_{\text{proj}}$ which is $-y$ direction.

In the center of the rapidity frame of $p + A$ collisions, the proton has rapidity Y_L and interacts at a transverse impact parameter \mathbf{r}_T with $N_{\text{Part}}^A \approx \sigma_{NN} T_A(\mathbf{r}_T)$ nucleons with rapidity $-Y_L$, where $T_A(\mathbf{r}_T)$ is the thickness function or the number of nucleons per unit area

$$T_A(\mathbf{r}_T) = \int dz \rho_A(\mathbf{r}), \quad (1)$$

with $\mathbf{r} = (x, y, z)$, $\mathbf{r}_T = (x, y)$, ρ_A is the number density of nucleons in the nucleus, σ_{NN} is the inelastic cross section of nucleon-nucleon collisions, and $Y_L \approx \ln[\sqrt{s}/(2m_N)]$ is the largest rapidity. The triangular rapidity distribution of hadrons is the result of string fragmentation between the projectile proton and the target nucleus. The hadrons produced by the wounded projectile proton are in the rapidity range $Y \in [0, Y_L]$, while those produced by the wounded target nucleons are in the range $Y \in [-Y_L, 0]$. The rapidity distribution of produced hadrons is approximately given by the BGK model [26] as

$$\frac{d^3 N_{pA}}{d^2 \mathbf{r}_T dY} = \frac{dN_{pp}}{dY} \left[T_A(\mathbf{r}_T) \frac{Y_L - Y}{2Y_L} + T_p \frac{Y_L + Y}{2Y_L} \right], \quad (2)$$

where $T_p \approx 1$ is the number of projectile protons per unit area. In the forward or projectile region $Y \approx Y_L$ the rapidity distribution approaches that of $p+p$ collisions dN_{pp}/dY , while in the backward or target region it approaches $(dN_{pp}/dY)T_A(\mathbf{r}_T)$. From experimental data we take a Gaussian form for dN_{pp}/dY ,

$$\frac{dN_{pp}}{dY} = a_1 \exp\left(-\frac{Y^2}{a_2}\right) \frac{1}{\sqrt{1 + a_3(\cosh Y)^4}}, \quad (3)$$

where a_1, a_2, a_3 are parameters. The values of these parameters in inelastic non-diffractive events in $p+p$ collisions at some collision energies are determined from the simulation of PYTHIA8.2 [27] and are listed in Table I.

Table I: The values of parameters in the hadron rapidity distribution in inelastic non-diffractive events in p+p collisions at various collision energies from the simulation of PYTHIA8.2 [27].

$\sqrt{s_{NN}}$ (GeV)	200	130	62.4	54.4	39
a_1	4.584	4.096	3.862	3.726	3.420
a_2	26.112	25.896	18.911	18.931	18.779
a_3	9.70×10^{-8}	5.61×10^{-7}	9.75×10^{-6}	1.71×10^{-5}	6.61×10^{-5}
$\sqrt{s_{NN}}$ (GeV)	27	19.6	14.5	11.5	7.7
a_1	3.421	3.099	3.049	2.784	2.831
a_2	13.555	13.629	9.947	10.488	8.008
a_3	2.50×10^{-4}	8.76×10^{-4}	2.44×10^{-3}	5.90×10^{-3}	9.40×10^{-3}

Such a trapezoidal shape of the rapidity distribution in (2) in the BGK model is a consequence of the string fragmentation and can be described naturally by the LUND string [28] and HIJING model [29, 30]. An extension of the BGK model has been applied to the jet tomography of twisted strongly-coupled quark-gluon plasmas [31] as well as the global polarization in nucleus-nucleus collisions [4]. In nucleus-nucleus collisions with projectile A and target B , at the point $\mathbf{r}_T = (x, y)$ in the transverse plane in the participant region (the coordinate system is shown in the upper-left of Fig. 1), the rapidity distribution of produced hadrons has the form which is a generalization of Eq. (2), i.e. the sum over contributions from projectile ('proj') and target ('tar')

$$\begin{aligned} \frac{d^3 N_{AB}}{d^2 \mathbf{r}_T dY} &= \frac{d^3 N_A^{\text{proj}}}{d^2 \mathbf{r}_T dY} + \frac{d^3 N_B^{\text{tar}}}{d^2 \mathbf{r}_T dY} \\ &= \frac{dN_{\text{pp}}}{dY} \left[T_A(\mathbf{r}_T - \mathbf{b}/2) \frac{Y_L + Y}{2Y_L} + T_B(\mathbf{r}_T + \mathbf{b}/2) \frac{Y_L - Y}{2Y_L} \right]. \end{aligned} \quad (4)$$

Here, thickness functions $T_A(\mathbf{r}_T - \mathbf{b}/2)$ and $T_B(\mathbf{r}_T + \mathbf{b}/2)$ in Eq. (4) are given by

$$T_{A,B}(\mathbf{r}_T \mp \mathbf{b}/2) = \int dz \rho^{A,B}(\mathbf{r}_T \mp \mathbf{b}/2), \quad (5)$$

where $\rho^{A,B}(\mathbf{r}_T \mp \mathbf{b}/2)$ the participant nucleon number density functions of nuclei A and B . One can check that the distribution (4) is proportional to $T_{A/B}(\mathbf{r}_T \mp \mathbf{b}/2)$ at the $Y = \pm Y_L$.

From Eq. (4) we can derive the distribution in the in-plane position x and the rapidity Y by integrating over the out-plane position y in the range $[-y_m, y_m]$,

$$\begin{aligned} \frac{d^2 N_{AB}}{dx dY} &= \frac{dN_{\text{pp}}}{dY} \left\{ \frac{1}{2} \int_{-y_m}^{y_m} dy [T_A(\mathbf{r}_T - \mathbf{b}/2) + T_B(\mathbf{r}_T + \mathbf{b}/2)] \right. \\ &\quad \left. + \frac{Y}{2Y_L} \int_{-y_m}^{y_m} dy [T_A(\mathbf{r}_T - \mathbf{b}/2) - T_B(\mathbf{r}_T + \mathbf{b}/2)] \right\}, \end{aligned} \quad (6)$$

where y_m is the maximum of y at a specific x , in the hard sphere model of the nuclear density distribution it is defined by the boundary of the overlapping region of two nuclei, while in the Woods-Saxon model there is no sharp boundary but it can be set to a value much larger than y_m in the hard sphere model. We define the normalized probability distribution of Y at x ,

$$f(Y, x) = \left(\frac{dN_{AB}}{dx} \right)^{-1} \frac{d^2 N_{AB}}{dx dY}, \quad (7)$$

where the distribution dN_{AB}/dx is given by

$$\begin{aligned} \frac{dN_{AB}}{dx} &= \int_{-Y_L}^{Y_L} dY \frac{d^2 N_{AB}}{dx dY} \\ &= \int_0^{Y_L} dY \frac{dN_{\text{pp}}}{dY} \int_{-y_m}^{y_m} dy [T_B(\mathbf{r}_T + \mathbf{b}/2) + T_A(\mathbf{r}_T - \mathbf{b}/2)]. \end{aligned} \quad (8)$$

According to the Bjorken scaling model [25], the average rapidity of the particle as a function of Y at x in the rapidity window $[Y - \Delta_Y/2, Y + \Delta_Y/2]$ is given by

$$\begin{aligned}\langle Y \rangle_\Delta &= \frac{\int_{Y-\Delta_Y/2}^{Y+\Delta_Y/2} dY' Y' f(Y', x)}{\int_{Y-\Delta_Y/2}^{Y+\Delta_Y/2} dY' f(Y', x)} \\ &\approx Y + \frac{\Delta_Y^2}{12} \frac{1}{f(Y, x)} \frac{df(Y, x)}{dY},\end{aligned}\quad (9)$$

where Δ_Y is the width of the rapidity window in which particles interact to reach collectivity. We assumed $\Delta_Y \ll Y$ so Δ_Y can be treated as a perturbation. The average rapidity of the particle as a function of x in the full rapidity range reads

$$\begin{aligned}\langle Y \rangle &= \frac{\int_{-Y_L}^{Y_L} dY Y f(Y, x)}{\int_{-Y_L}^{Y_L} dY f(Y, x)} \\ &= \frac{1}{Y_L} \langle Y^2 \rangle_{\text{pp}} \frac{\int_{-y_m}^{y_m} dy [T_A(\mathbf{r}_T - \mathbf{b}/2) - T_B(\mathbf{r}_T + \mathbf{b}/2)]}{\int_{-y_m}^{y_m} dy [T_A(\mathbf{r}_T - \mathbf{b}/2) + T_B(\mathbf{r}_T + \mathbf{b}/2)]},\end{aligned}\quad (10)$$

where $\langle Y^2 \rangle_{\text{pp}}$ is defined as

$$\langle Y^2 \rangle_{\text{pp}} = \frac{\int_{-Y_L}^{Y_L} dY (dN_{\text{pp}}/dY) Y^2}{\int_{-Y_L}^{Y_L} dY (dN_{\text{pp}}/dY)}.\quad (11)$$

The average longitudinal momentum p_z and the average energy E_p of the particle are

$$\begin{aligned}\langle p_z \rangle &= \langle p_T \rangle \sinh \langle Y \rangle_\Delta \\ &\approx \langle p_T \rangle \sinh Y + \langle p_T \rangle \frac{\Delta_Y^2}{12} \frac{d \ln f(Y, x)}{dY} \cosh Y, \\ \langle E_p \rangle &= \langle p_T \rangle \cosh \langle Y \rangle_\Delta \\ &\approx \langle p_T \rangle \cosh Y + \langle p_T \rangle \frac{\Delta_Y^2}{12} \frac{d \ln f(Y, x)}{dY} \sinh Y,\end{aligned}\quad (12)$$

where we have treated terms proportional to Δ_Y^2 as a perturbation. At a given Y we consider two particles located at $x + \Delta x/2$ and $x - \Delta x/2$, in their center of mass frame, the local average OAM for two colliding particles is given by [25]

$$\begin{aligned}\langle L_y \rangle &\approx -(\Delta x) \langle p_z^{\text{cm}} \rangle \\ &\approx -(\Delta x)^2 \langle p_T \rangle \frac{\Delta_Y^2}{24} \frac{d \ln f(Y, x)}{dY dx},\end{aligned}\quad (13)$$

where $\langle p_z^{\text{cm}} \rangle$ is the average longitudinal momentum in the center of mass frame for one particle. Here Δx is a typical impact parameter of particle scatterings. In following sections we will use the average of $d \ln f(Y, x)/dx dY$ over the in-plane coordinate

$$\left\langle \frac{d \ln f(Y, x)}{dY dx} \right\rangle = \frac{\int dx (dN_{AB}/dx dY) (d \ln f(Y, x)/dY dx)}{\int dx (dN_{AB}/dx dY)},\quad (14)$$

where $dN_{AB}/dx dY$ is given in Eq. (6) as a weight function.

III. RAPIDITY DISTRIBUTIONS OF HADRONS IN HARD SPHERE AND WOODS-SAXON MODEL

In this section we will calculate the rapidity distributions for hadrons $f(Y, x)$ in Eq. (7) with the hard sphere (HS) and Woods-Saxon (WS) nuclear density distribution, which are involved in the thickness functions in Eq. (5). As a simple illustration, we consider collisions of two identical nuclei with nucleon number A .

A. Hard sphere nuclear density distribution

The HS nuclear density is given by

$$\rho_{\text{HS}}(\mathbf{r}) = \frac{3A}{4\pi R_A^3} \theta(R_A - r), \quad (15)$$

where $R_A = 1.2A^{1/3}$ fm is the nucleus radius. The thickness functions have the analytical form

$$T_A(\mathbf{r}_T \pm \mathbf{b}/2) = \frac{6A}{4\pi R_A^3} [R_A^2 - (x \pm b/2)^2 - y^2]^{1/2}. \quad (16)$$

Inserting the above into Eq. (4), we obtain the hadron distribution $dN_{AA}/(dxdy dY)$, whose numerical results are shown in Fig. 2 at three rapidity values in Au+Au collisions at $\sqrt{s_{NN}} = 200$ GeV with the impact parameter $b = 1.2R_A$. In the HS model, the overlapping region of two nuclei is limited by $|x| < R_A - b/2$ and $|y| < \sqrt{R_A^2 - (|x| + b/2)^2}$. We see that the distribution at $Y = 0$ is symmetric in x and y while that the distribution in the forward (backward) rapidity is shifted to the right (left) in x direction.

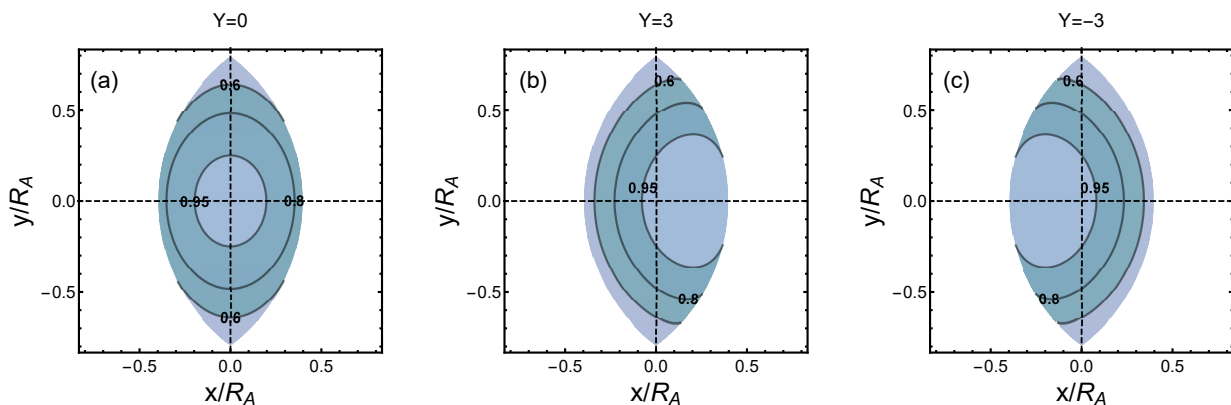


Figure 2: The hadron distributions (contour plot) in the HS model in the transverse plane for Au+Au collisions at $\sqrt{s_{NN}} = 200$ GeV and $b = 1.2R_A$. The number on the contour line denotes the value on the line normalized by that at the origin. The rapidity values are chosen to be $Y = 0$ (central), $Y = 3$ (forward) and $Y = -3$ (backward).

Integrating over the out-plane coordinate y , we obtain the hadron distribution function

$$\frac{d^2 N_{AA}}{dxdY} = \frac{6A}{4\pi R_A^3} \frac{dN_{pp}}{dY} \left[C_1^+ + C_1^- + \frac{Y}{Y_L} (C_1^+ - C_1^-) \right], \quad (17)$$

where C_1^\pm are defined in Eq. (A1). In Fig. 3(a), we show $dN_{AA}/dxdY$ as functions of in-plane coordinate x at various rapidity values. We see that the distribution at $Y = 0$ is symmetric while the distribution at forward (backward) rapidity is shifted to the positive (negative) x . The magnitude of the shift increases slightly with the rapidity. In Fig. 3(b), we show $dN_{AA}/dxdY$ as functions of the rapidity at different x . We see that the distribution at $x = 0$ is symmetric while that at positive (negative) x is tilted to the forward (backward) rapidity. From Eq. (7), we obtain the normalized function $f(Y, x)$ as

$$f(Y, x) = \frac{dN_{pp}/dY}{2 \int_0^{Y_L} dY (dN_{pp}/dY)} \left(1 + \frac{Y}{Y_L} \cdot \frac{C_1^+ - C_1^-}{C_1^+ + C_1^-} \right), \quad (18)$$

where $|x| \leq R_A - b/2$ and $b \leq 2R_A$. The numerical results of $f(Y, x)$ are shown in Fig. 3(c,d).

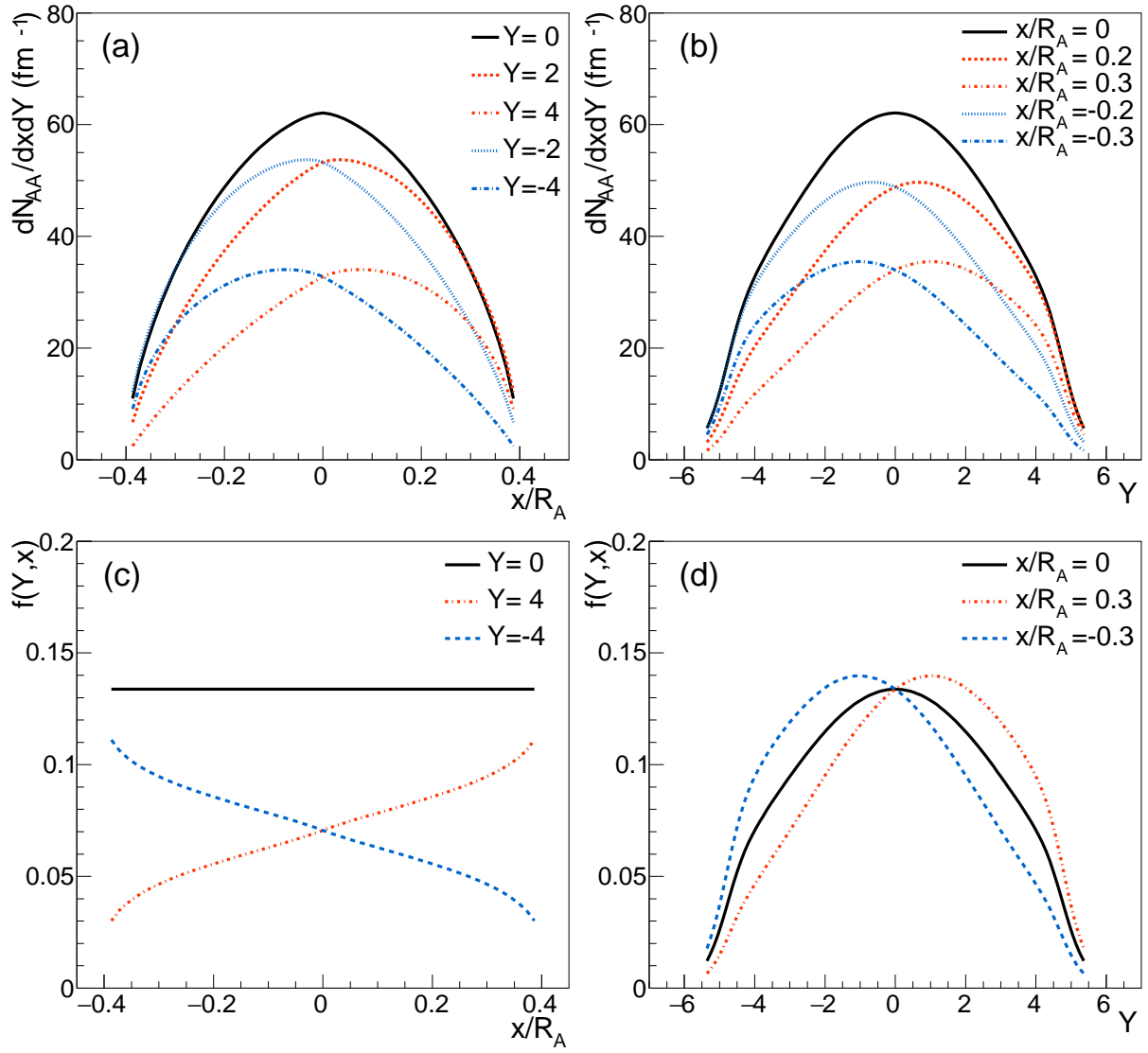


Figure 3: The hadron distributions in the HS model in Au+Au collisions at $\sqrt{s_{NN}} = 200$ GeV as functions of (a) the in-plane position x at different rapidity values and as functions of (b) the rapidity Y at different values of x . The impact parameter is set to $b = 1.2R_A$. (c) The normalized distribution $f(Y, x)$ as functions of x at different Y . (d) The normalized distribution $f(Y, x)$ corresponding to (b). The definition of $f(Y, x)$ is given in Eq. (18).

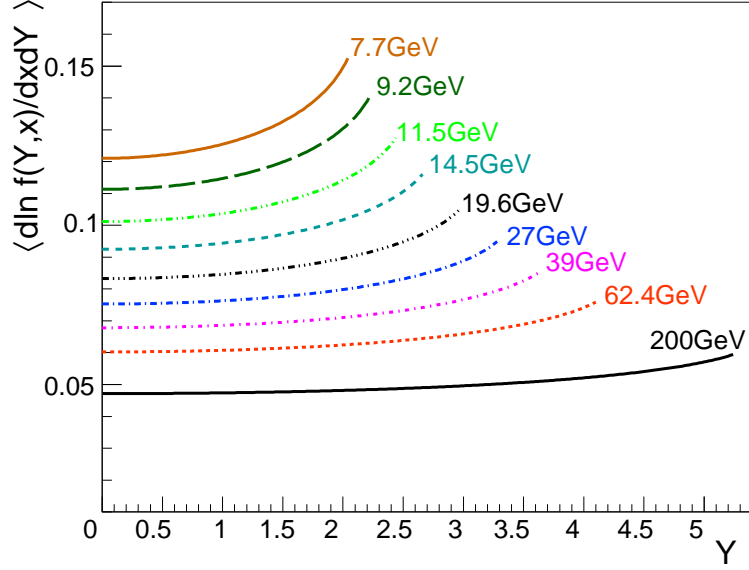


Figure 4: The average quantity $\langle d \ln f(Y, x) / dx dY \rangle$ as functions of the rapidity Y in the HS model for Au+Au collisions at various collision energies. The impact parameter is set to $b = 1.2R_A$.

The derivative of $\ln f(Y, x)$ with respect to Y and x is derived in Eq. (A10), from which one can obtain $\langle d \ln f(Y, x) / dx dY \rangle$ through Eq. (14). We show the numerical results of $\langle d \ln f(Y, x) / dx dY \rangle$ in Fig. 4 as rapidity functions in Au+Au collisions at various collision energies. We see that $\langle d \ln f(Y, x) / dx dY \rangle$ increases slowly with the rapidity via the Y/Y_L term which can be seen in Eq. (A10). The relatively obvious increase in the forward rapidity region is an artifact of the HS model in comparison with the WS model in the next subsection. The energy dependence of $\langle d \ln f(Y, x) / dx dY \rangle$ is mainly controlled by $Y_L \approx \ln[\sqrt{s}/(2m_N)]$ as shown in Eq. (A10).

From Eq. (10) we obtain the average rapidity in the full rapidity range as

$$\langle Y \rangle = \frac{1}{Y_L} \langle Y^2 \rangle_{\text{PP}} \frac{C_1^+ - C_1^-}{C_1^+ + C_1^-}. \quad (19)$$

The numerical result of the above average rapidity is shown in Fig. 5 which is consistent with Fig. 5 of Ref. [25].

B. Woods-Saxon nuclear density distribution

In this subsection we choose a more realistic nuclear density distribution, the WS distribution, defined as

$$f_{\text{WS}}(\mathbf{r}) = \frac{C_0}{\exp[(r - R_A)/a] + 1}, \quad (20)$$

where $r = |\mathbf{r}|$, $a = 0.54$ fm, and C_0 is a normalization constant to make the volume integral of $f_{\text{WS}}(\mathbf{r})$ to be the number of nucleons in the nucleus,

$$C_0 = \frac{A}{4\pi} \left[\int_0^\infty dr r^2 \frac{1}{\exp[(r - R_A)/a] + 1} \right]^{-1}. \quad (21)$$

For Au-197 nuclei, we have $R_A \approx 6.98$ fm, $C_0 \approx A/(4\pi)/120.2 \approx 0.131$ fm⁻³. According to the Glauber model, the participant nucleon number density for two colliding nuclei are given by

$$\begin{aligned} \rho_{\text{WS}}^{A,B}(\mathbf{r}_T \mp \mathbf{b}/2) &= f_{\text{WS}}^{A,B}(\mathbf{r}_T \mp \mathbf{b}/2) \\ &\times \left\{ 1 - \exp \left[-\sigma_{NN} \int dz f_{\text{WS}}^{B,A}(\mathbf{r}_T \pm \mathbf{b}/2) \right] \right\}, \end{aligned} \quad (22)$$

where σ_{NN} can be taken as the inelastic pp collision cross section.

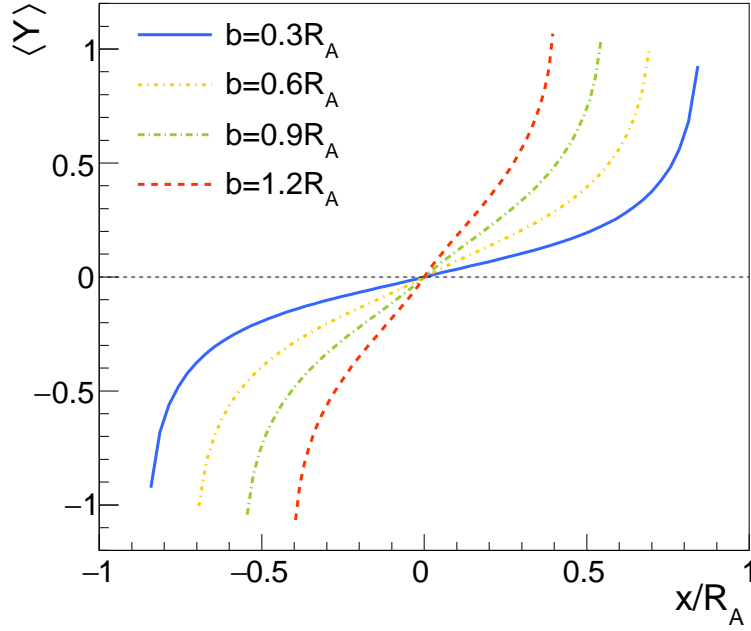


Figure 5: The average rapidity in the full rapidity range for Au+Au collisions at $\sqrt{s_{NN}} = 200$ GeV as functions of x from Eq. (19) in the HS model.

We consider collisions of two identical nuclei. With the WS distribution in Eq. (20), we can calculate $f(Y, x)$ in Eq. (7). From Eq. (5), the thickness functions become

$$\begin{aligned}
 T_A(\mathbf{r}_T \pm \mathbf{b}/2) &= \int_{-\infty}^{\infty} dz \rho_{\text{WS}}^A(\mathbf{r}_T \pm \mathbf{b}/2) \\
 &= \int_{-\infty}^{\infty} dz f_{\text{WS}}(\mathbf{r}_T \pm \mathbf{b}/2) \\
 &\quad \times \left\{ 1 - \exp \left[-\sigma_{NN} \int dz f_{\text{WS}}(\mathbf{r}_T \mp \mathbf{b}/2) \right] \right\}.
 \end{aligned} \tag{23}$$

Substituting Eq. (23) into Eq. (4) and (6), we obtain the hadron distribution $dN_{AA}/(dx dy dY)$ in xy plane and $dN_{AA}/(dx dY)$ by an integration over y , respectively. The numerical results for $dN_{AA}/(dx dy dY)$ and $dN_{AA}/(dx dY)$ are shown in Fig. 6 and 7 respectively for different rapidity values in Au+Au collisions at 200 GeV with $b = 1.2R_A$. Similar to results of the HS model in Fig. 2 and (3), in the forward/backward rapidity region, the hadron distributions are tilted toward the positive/negative x . But different from results of the HS model, the hadron distributions in the WS model are smooth in the edge of the overlapping region.

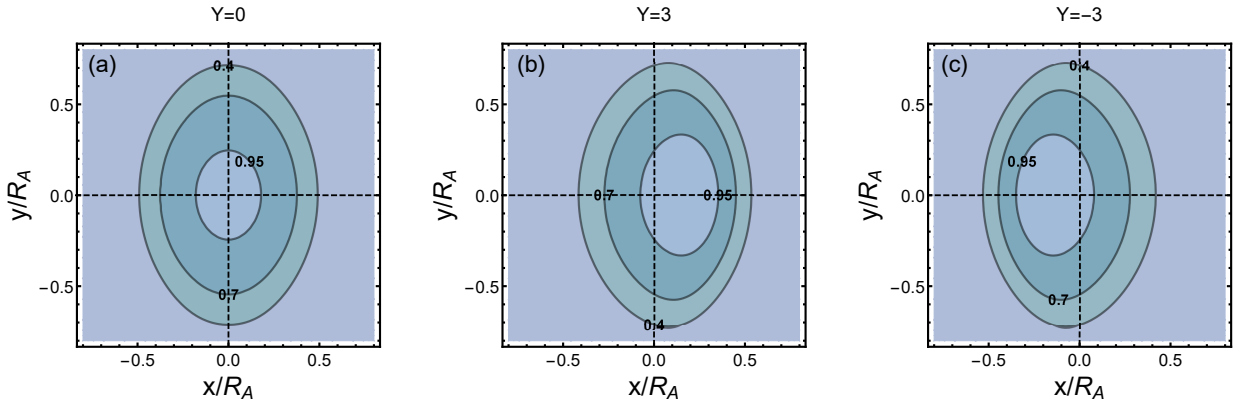


Figure 6: The hadron distributions (contour plot) in the WS model in the transverse plane for Au+Au collisions at $\sqrt{s_{NN}} = 200$ GeV and $b = 1.2R_A$. The number on the contour line denotes the value on the line normalized by that at the origin. The rapidity values are chosen to be $Y = 0$ (central), $Y = 3$ (forward) and $Y = -3$ (backward).

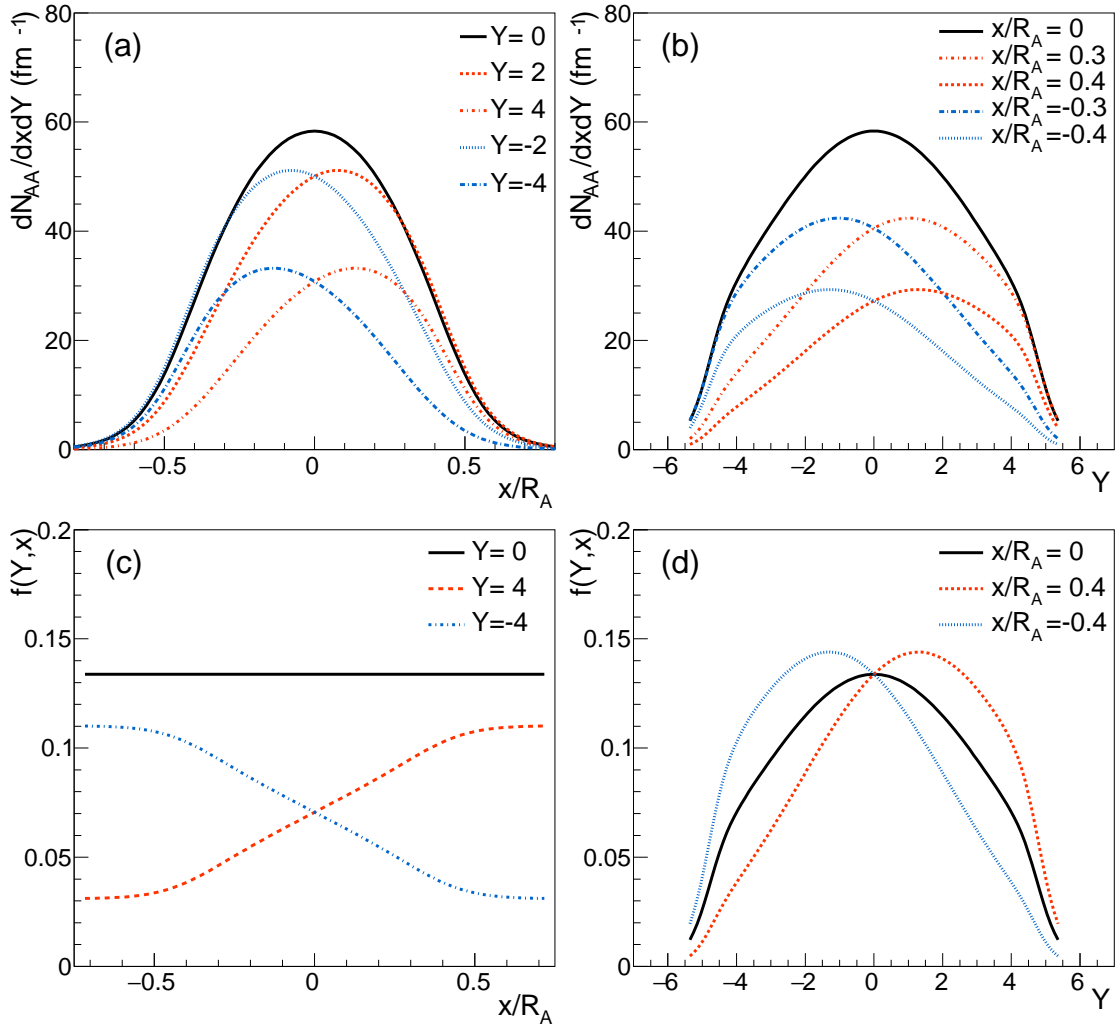


Figure 7: The hadron distributions in the WS model in Au+Au collisions at $\sqrt{s_{NN}} = 200$ GeV as functions of (a) the in-plane position x at different rapidity values and as functions of (b) the rapidity Y at different values of x . The impact parameter is set to $b = 1.2R_A$. (c) The normalized distribution $f(Y, x)$ as functions of x at different Y . (d) The normalized distribution $f(Y, x)$ corresponding to (b). The definition of $f(Y, x)$ is given in Eq. (7).

We show in Fig. 8 the numerical results for $\langle d \ln f(Y, x) / dY dx \rangle$ applying Eq. (14) to the WS model. We choose $b = 1.2R_A$ in Au+Au collisions at different collision energies. We choose σ_{NN} as the inelastic proton-proton cross section determined by the global fit of the experimental data [32], whose values are listed in Table II. Also shown in Table II are the values of $\langle d \ln f(Y, x) / dY dx \rangle$ at $Y = 0$ in Au+Au collisions with the HS and WS distribution.

Table II: The inelastic nucleon-nucleon cross section σ_{NN} at different collisions energies (first two rows). The numerical results of $\langle d \ln f(Y, x) / dY dx \rangle$ at $Y = 0$ in Au+Au collisions at different collisions energies (last two rows). The impact parameter is set to $b = 1.2R_A$ corresponding to 20-50% centrality in experiments.

$\sqrt{s_{NN}}$ (GeV)	200	62.4	54.4	39	27	19.6	14.5	11.5	9.2	7.7
σ_{NN} (mb)	42.0	36.3	35.2	33.6	32.8	32.3	31.8	31.4	30.9	30.6
$\langle \frac{d \ln f(Y, x)}{dY dx} \rangle_{\text{HS}}$	0.0471	0.0602	0.0622	0.0678	0.0753	0.0833	0.0925	0.101	0.111	0.121
$\langle \frac{d \ln f(Y, x)}{dY dx} \rangle_{\text{WS}}$	0.0374	0.0460	0.0472	0.0507	0.0558	0.0614	0.0678	0.0739	0.0809	0.0876

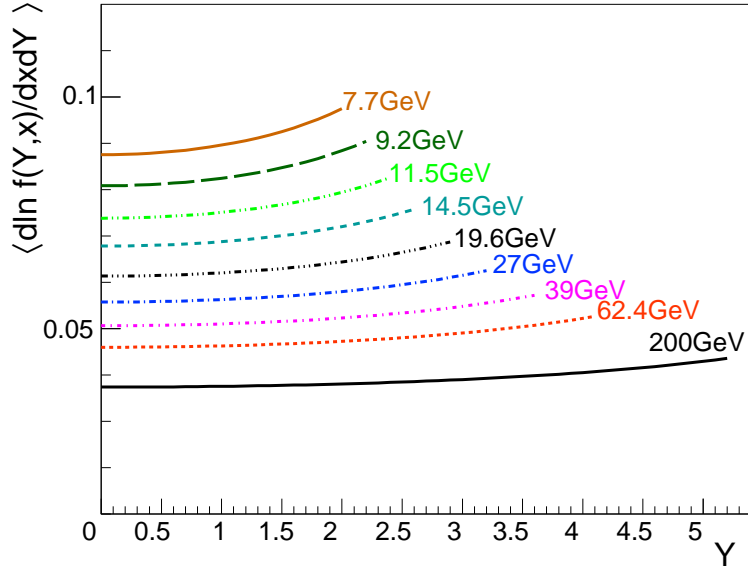


Figure 8: The average quantity $\langle d \ln f(Y, x) / dY dx \rangle$ as functions of the rapidity Y in the WS model for Au+Au collisions at various collision energies. The impact parameter is set to $b = 1.2R_A$.

Similar to the results of the HS model, $\langle d \ln f(Y, x) / dY dx \rangle$ at $Y = 0$ increases with decreasing collision energies, and it is a slowly increasing function of Y . There are also some differences between the WS and HS results. First, due to the smooth function in the WS model at the edge of the nucleus, the rapidity dependence of $\langle d \ln f(Y, x) / dY dx \rangle$ in the WS model is slightly weaker than that in the HS model. Second, besides the explicit collision energy dependence of Y_L , σ_{NN} also depends on the collision energy and enters the thickness function via Eq. (22), therefore the increase of $\langle d \ln f(Y, x) / dY dx \rangle$ at $Y = 0$ in the WS model with the decreasing collision energy is slightly slower than in the HS model.

The numerical result for the average rapidity in the full rapidity range from Eq. (10) is shown in Fig. 9 which is consistent with Fig. 5 of Ref. [25]. The difference between Fig. 9 with the WS distribution and Fig. 5 with the HS distribution is that in the edge of the overlapping region of two nuclei $\langle Y \rangle$ with the WS distribution is smoothly vanishing far outside the overlapping region but $\langle Y \rangle$ with the HS distribution is discontinuous at the boundary.

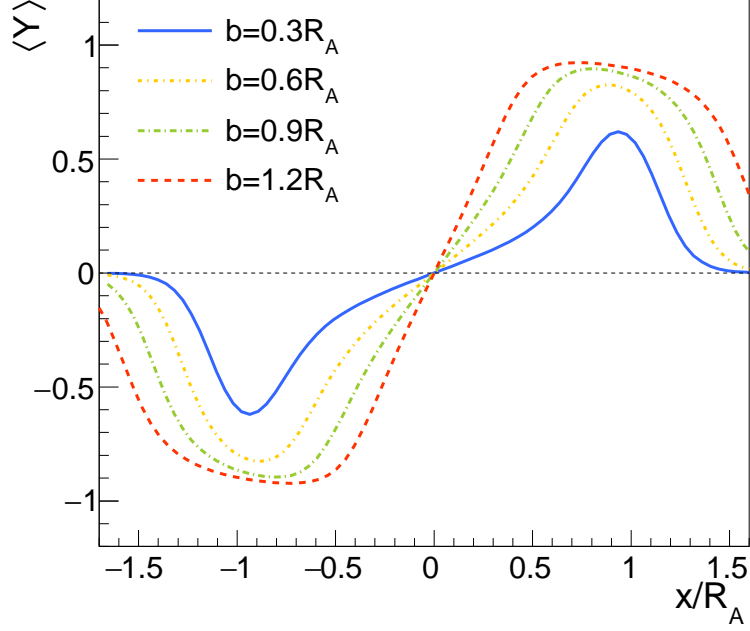


Figure 9: The average rapidity in the full rapidity range for Au+Au collisions $\sqrt{s_{NN}} = 200$ GeV as a function of x from Eq. (10) in the WS model.

IV. POLARIZATION INDUCED BY ORBITAL ANGULAR MOMENTUM

As proposed in [25], the OAM in peripheral collisions of two nuclei can induce hadron polarization. Here we assume that the polarization is proportional the local OAM

$$\begin{aligned}
 P_q(Y) &= \alpha(Y) \langle L_y \rangle \\
 &= -\alpha(Y) (\Delta x)^2 \frac{\Delta_Y^2}{24} \langle p_T \rangle \left\langle \frac{d \ln f(Y, x)}{dY dx} \right\rangle,
 \end{aligned} \tag{24}$$

where we have replaced $d \ln f(Y, x)/dY dx$ in Eq. (13) with its average in Eq. (14), and $\alpha(Y)$ is a rapidity-dependent coefficient. The minus sign means that the polarization is along $-y$ direction. We define a parameter $\kappa(Y) = \alpha(Y) (\Delta x)^2 \Delta_Y^2$ as a function of the rapidity Y . Note that Δx , Δ_Y and $\langle p_T \rangle$ can also depend on Y in principle.

The global polarization of Λ hyperons at mid-rapidity has been measured in the STAR experiment by which the parameters in Eq. (24) can be determined. At mid-rapidity $Y = 0$, Eq. (24) becomes

$$P_q(Y = 0) = -\frac{1}{24} \kappa_0 \langle p_T \rangle \left\langle \frac{d \ln f(Y, x)}{dY dx} \right\rangle_{Y=0}, \tag{25}$$

where we have combined three parameters into one $\kappa_0 \equiv \kappa(0)$. The average transverse momentum $\langle p_T \rangle$ can be determined by kaon data available at some collision energies and an interpolation is made for other collision energies. Results of $\langle d \ln f(Y, x)/dY dx \rangle_{Y=0}$ are already shown in Table II.

As our first option, we assume that the parameter κ_0 is a constant of the collision energy whose value is chosen to describe via Eq. (25) the polarization data in the energy range 7.7-62.4 GeV. The results are shown in the left panel of Fig. 10. We see that the collision energy dependence of $P_q(Y = 0)$ in HS with $\kappa_0 = 6.4$ and that in WS with $\kappa_0 = 8.4$ are roughly consistent with the polarization data in the energy range 7.7-62.4 GeV. But the fitting curves are larger than the data of 200 GeV. Interestingly we find that the energy dependence of our results in both HS and WS model can be well fitted by $\sim 1/Y_L$ (dashed line). As our second option, we use the energy dependent κ_0 to fit the data in the energy range 7.7-62.4 GeV including 200 GeV. The results are shown in the right panel of Fig. 10.

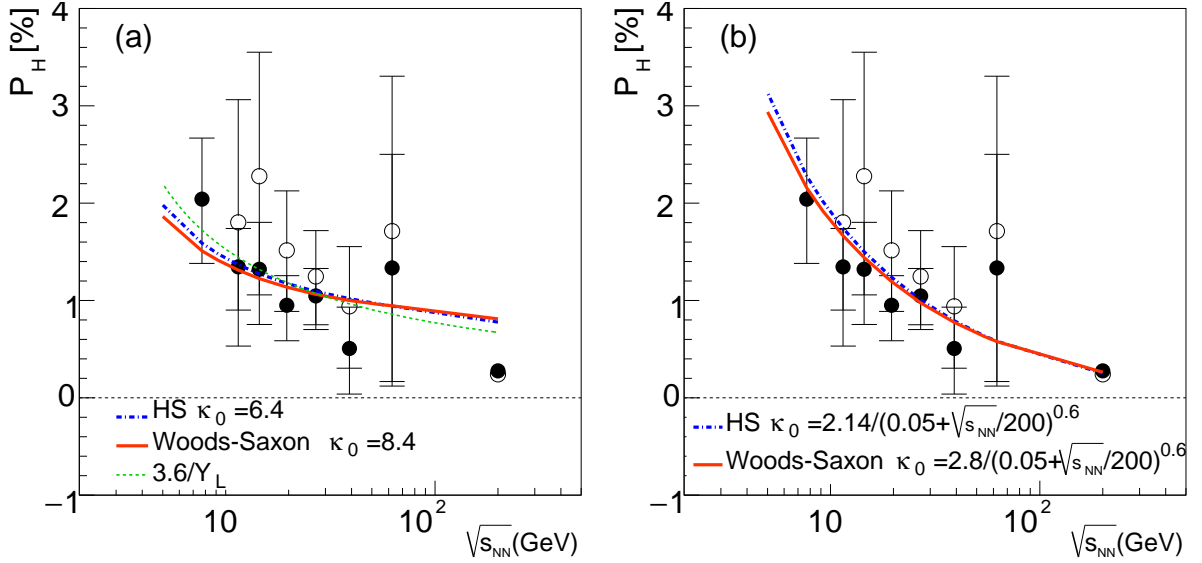


Figure 10: The global polarization of Λ and $\bar{\Lambda}$ at mid-rapidity in the HS and WS model in Au+Au collisions at different collision energies. The impact parameter is set to $b = 1.2R_A$ corresponding to the centrality 20-50%. The STAR data are represented by the solid (Λ) and open ($\bar{\Lambda}$) circle [13, 14]. (a) κ_0 is a constant of the collision energy. (b) κ_0 depends on the collision energy.

Once the values of κ_0 are constrained by the polarization data at mid-rapidity, we can predict the polarization of Λ hyperons at larger rapidity. In our prediction we take the WS model and the energy dependent κ_0 as determined in the right panel of Fig. 10. Since we do not know the rapidity dependence of $\kappa(Y)$ and $\langle p_T \rangle$ we will consider three cases and make corresponding prediction for the rapidity dependence of the global polarization: (a) Both $\kappa(Y) = \kappa_0$ and $\langle p_T \rangle$ are taken to be constants in rapidity. Therefore the rapidity dependence of the global polarization is solely from $\langle d \ln f(Y, x) / dY dx \rangle$. (b) Only $\kappa(Y) = \kappa_0$ is assumed to be constant in rapidity while $\langle p_T \rangle$ depends on the rapidity. The mid-rapidity values of $\langle p_T \rangle$ are taken from the kaon data in Au+Au collisions in the collision energy range 7.7-200 GeV [33, 34]. The rapidity dependence of $\langle p_T \rangle$ is given by fitting the kaon data in Au+Au collisions at 62.4 GeV and 200 GeV [35, 36]. (c) A rapidity constant $\langle p_T \rangle$ is adopted which takes its value at mid-rapidity at each energy, but the rapidity dependence of $\kappa(Y)$ is assumed to take the form in Eq. (B4). (d) Both $\kappa(Y)$ and $\langle p_T \rangle$ depend on the rapidity. The rapidity dependence of $\langle p_T \rangle$ is the same as case (b), while the rapidity dependence of $\kappa(Y)$ is the same as case (c).

Figure 11(a-d) show the polarization results for case (a-d) respectively. In Fig. 11(a) for the constant κ and $\langle p_T \rangle$ in rapidity we see that the polarization increases slightly with Y at each collision energy. The positive slope in rapidity (the increase rate of the polarization per unit rapidity) decreases with the collision energy. Figure 11(b) shows the polarization results for the constant κ and rapidity dependent $\langle p_T \rangle$. We see that the polarization decreases with Y at each collision energy. At lower energies the decreasing slope (the absolute value of the slope) is larger than that at higher energies. At 200 GeV the polarization is almost a constant of rapidity. In Fig. 11(c) for the rapidity dependent κ and constant $\langle p_T \rangle$ in rapidity we see that the polarization increases with rapidity. The lower the collision energy the larger the increasing slope is. The increase trend is stronger than in case (a) and (d) at the same collision energy. Figure 11(d) shows the polarization results for the rapidity dependent κ and $\langle p_T \rangle$. At high energies the polarizations increase weakly with rapidity while they are almost constants of rapidity at low energies. Note that the form of $\kappa(Y)$ in Eq. (B4) used in case (c) and (d) is valid for $\mu_B \lesssim 0.45$ GeV, however, it is beyond such a μ_B limit at 7.7 GeV. Therefore the curves of 7.7 GeV in Figs. 11(c,d) are not shown since they are not reliable.

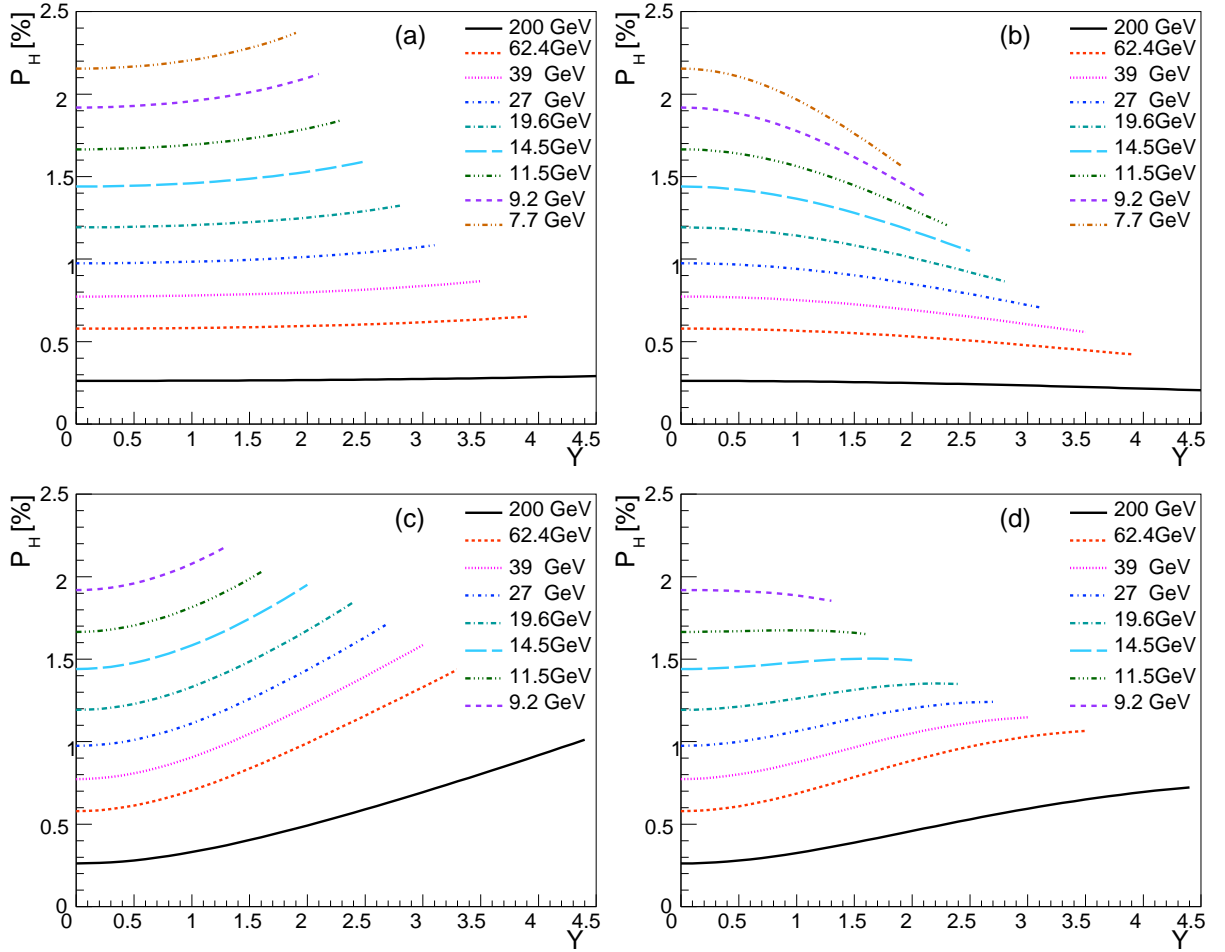


Figure 11: The polarization of Λ and $\bar{\Lambda}$ in the WS model as functions of rapidity in Au+Au collisions at different collision energies. We use the collision energy dependent κ_0 as as determined in the right panel of Fig. 10. The impact parameter is set to $b = 1.2R_A$ corresponding to the centrality 20-50%. The results in case (a), (b), (c) and (d) are presented in panel (a), (b), (c) and (d) respectively.

V. SUMMARY

We propose a geometric model for the hadron polarization in heavy ion collisions with an emphasis on the rapidity dependence. It is based on the model of Brodsky, Gunion, and Kuhn and that of the Bjorken scaling [25]. The starting point is the hadron rapidity distribution $d^3N_{AA}/d^2\mathbf{r}_T dY$ as a function of the transverse position \mathbf{r}_T in the overlapping region of colliding nuclei and the rapidity Y . We use the hard sphere and Woods-Saxon model for the nuclear density distribution from which the thickness function is obtained. The rapidity distribution $d^3N_{AA}/dx dY$ depending on the in-plane position x in the overlapping region can be derived from $d^3N_{AA}/d^2\mathbf{r}_T dY$ by integration over the out-plane position y . The average rapidity of hadrons can be obtained from the normalized distribution $d^3N_{AA}/dx dY$ or $f(Y, x)$. The collective longitudinal momentum $\langle p_z \rangle$ is proportional to $d \ln f(Y, x)/dY$. Then the average local orbital angular momentum $\langle L_y \rangle$ is proportional to the average of $d \ln f(Y, x)/dx dY$ over x , which is a function of Y . The hadron polarization is assumed to be proportional to $\alpha(Y) \langle L_y \rangle$ with $\alpha(Y)$ is an unknown rapidity function representing a transfer coefficient from the orbital angular momentum in the initial state to the hadron polarization in the final state. There are two parameters in our model that can have rapidity dependence. These parameters at mid-rapidity can be constrained by the polarization data of Λ and $\bar{\Lambda}$. Finally we make predictions for the rapidity dependence of the hadron polarization in the collision energy range 7.7-200 GeV by taking a few assumed forms of the parameters. The predictions can be tested by future experiments.

Acknowledgments

The authors thanks C.M. Ko and J.Y. Jia for insightful discussions. ZTL and QW are supported in part by the National Natural Science Foundation of China (NSFC) under Grant No. 11890713 and No. 11535012.

Appendix A: Derivation of $d \ln f(Y, x)/dY dx$ for hard sphere distribution

In this Appendix we will derive $d \ln f(Y, x)/dY dx$ in the HS model for the nuclear density distribution from Eq. (17) and (18). The definition of C_1^\pm and C_2^\pm are

$$C_1^\pm = \int_0^{y_m} dy [R_A^2 - (x \mp b/2)^2 - y^2]^{1/2}, \quad (\text{A1})$$

$$C_2^\pm = \int_0^{y_m} dy [R_A^2 - (x \mp b/2)^2 - y^2]^{-1/2}, \quad (\text{A2})$$

where y_m is the maximum of y at a fixed x

$$y_m = [R_A^2 - (|x| + b/2)^2]^{1/2}. \quad (\text{A3})$$

The analytical expressions of C_1^\pm are

$$C_1^+(x) = \begin{cases} \frac{1}{2} \sqrt{R_A^2 - (x + b/2)^2} \sqrt{2bx} + I_-(x), & 0 < x < R_A - b/2 \\ \frac{\pi}{4} [R_A^2 - (x - b/2)^2], & -(R_A - b/2) < x \leq 0 \end{cases} \quad (\text{A4})$$

$$C_1^-(x) = \begin{cases} \frac{\pi}{4} [R_A^2 - (x + b/2)^2], & 0 \leq x < R_A - b/2 \\ \frac{1}{2} \sqrt{R_A^2 - (x - b/2)^2} \sqrt{-2bx} + I_+(x), & -(R_A - b/2) < x < 0 \end{cases} \quad (\text{A5})$$

where the function $I_\pm(x)$ are defined as

$$I_\pm(x) = \frac{1}{2} [R_A^2 - (x \pm b/2)^2] \arctan \frac{\sqrt{R_A^2 - (x \mp b/2)^2}}{\sqrt{\mp 2bx}} \quad (\text{A6})$$

The analytical expressions of C_2^\pm are

$$C_2^+(x) = \begin{cases} \arctan \frac{\sqrt{R_A^2 - (x + b/2)^2}}{\sqrt{2bx}}, & 0 < x < R_A - b/2 \\ \frac{\pi}{2}, & -(R_A - b/2) < x \leq 0 \end{cases} \quad (\text{A7})$$

$$C_2^-(x) = \begin{cases} \frac{\pi}{2}, & 0 \leq x < R_A - b/2 \\ \arctan \frac{\sqrt{R_A^2 - (x - b/2)^2}}{\sqrt{-2bx}}, & -(R_A - b/2) < x < 0 \end{cases} \quad (\text{A8})$$

In terms of C_1^\pm and C_2^\pm , we obtain the derivative of $\ln f(Y, x)$ with respect to Y as

$$\frac{d \ln f(Y, x)}{dY} = \frac{d \ln(dN_{pp}/dY)}{dY} + \frac{1}{Y} - \frac{1}{Y} \left\{ 1 + \frac{Y}{Y_L} \cdot \frac{C_1^+ - C_1^-}{C_1^+ + C_1^-} \right\}^{-1}, \quad (\text{A9})$$

and then the derivative of $d \ln f(Y, x)/dY$ with respect to x as

$$\begin{aligned} \frac{d \ln f(Y, x)}{dY dx} &= \frac{1}{Y_L} \left[1 + \frac{Y}{Y_L} \cdot \frac{C_1^+ - C_1^-}{C_1^+ + C_1^-} \right]^{-2} \left\{ -\frac{x(C_2^+ - C_2^-) - (b/2)(C_2^+ + C_2^-)}{(C_1^+ + C_1^-)} \right. \\ &\quad + \frac{(C_1^+ - C_1^-) [x(C_2^+ + C_2^-) - (b/2)(C_2^+ - C_2^-)]}{(C_1^+ + C_1^-)^2} \\ &\quad - 2(2b|x|)^{1/2} (|x| + b/2) [R_A^2 - (|x| + b/2)^2]^{-1/2} \\ &\quad \left. \times \frac{C_1^+ \theta(-x) + C_1^- \theta(x)}{(C_1^+ + C_1^-)^2} \right\}, \quad (\text{A10}) \end{aligned}$$

where we have used

$$\frac{d}{dx} \int_0^{a(x)} dy b(x, y) = \int_0^{a(x)} dy \frac{\partial b(x, y)}{\partial x} + b(x, a(x)) \frac{da(x)}{dx}. \quad (\text{A11})$$

Appendix B: Rapidity dependence of $\kappa(Y)$ in case (c) and (d)

There is a similarity in hadron production between the case at forward rapidity but high collision energy and that at central rapidity but lower collision energy. Here the baryon number density or baryon chemical potential is the relevant physical quantity. Therefore, if we neglect the system size effect, we can make an ansatz for $\kappa(Y)$ based on this similarity.

By fitting the data in Fig. 8(b) we find the following energy behavior of $\kappa_0 \equiv \kappa(Y = 0)$,

$$\kappa(Y = 0) = \frac{2.8}{(0.05 + \sqrt{s_{NN}}/200)^{0.6}}. \quad (\text{B1})$$

The collision energy dependence of the baryon chemical potential at mid-rapidity can be given by [37]

$$\mu_B(Y = 0) = \frac{1.3075}{1 + 0.288\sqrt{s_{NN}}} \text{ GeV}. \quad (\text{B2})$$

We can solve $\sqrt{s_{NN}}$ as a function of $\mu_B(Y = 0)$ and obtain

$$\kappa(Y = 0) = \frac{2.8}{(0.05 + (1.3075/\mu_B(Y = 0) - 1)/57.6)^{0.6}}. \quad (\text{B3})$$

within the range $\mu_B \lesssim 0.45$ GeV, i.e., in the collision energy range 7.7-200 GeV. We can generalize the above expression to other rapidity values as

$$\kappa(Y) = \frac{2.8}{(0.05 + (1.3075/\mu_B(Y) - 1)/57.6)^{0.6}}, \quad (\text{B4})$$

by taking the following parametrization of $\mu_B(Y)$ [38]

$$\mu_B(Y) = \mu_B(Y = 0) + w(\sqrt{s_{NN}}) Y^2, \quad (\text{B5})$$

with the width parameter

$$w(\sqrt{s_{NN}}) = 0.09527 - 0.01594 \log \sqrt{s_{NN}}. \quad (\text{B6})$$

-
- [1] Z.-T. Liang and X.-N. Wang, Phys. Rev. Lett. **94**, 102301 (2005), [Erratum: Phys. Rev. Lett.96,039901(2006)], nucl-th/0410079.
[2] Z.-T. Liang and X.-N. Wang, Phys. Lett. **B629**, 20 (2005), nucl-th/0411101.
[3] S. A. Voloshin (2004), nucl-th/0410089.
[4] B. Betz, M. Gyulassy, and G. Torrieri, Phys. Rev. **C76**, 044901 (2007), 0708.0035.
[5] F. Becattini, F. Piccinini, and J. Rizzo, Phys. Rev. **C77**, 024906 (2008), 0711.1253.
[6] F. Becattini, G. Inghirami, V. Rolando, A. Beraudo, L. Del Zanna, A. De Pace, M. Nardi, G. Pagliara, and V. Chandra, Eur. Phys. J. **C75**, 406 (2015), [Erratum: Eur. Phys. J.C78,no.5,354(2018)], 1501.04468.
[7] L.-G. Pang, H. Petersen, Q. Wang, and X.-N. Wang, Phys. Rev. Lett. **117**, 192301 (2016), 1605.04024.
[8] W.-T. Deng and X.-G. Huang, Phys. Rev. **C93**, 064907 (2016), 1603.06117.
[9] Y. Jiang, Z.-W. Lin, and J. Liao, Phys. Rev. **C94**, 044910 (2016), [Erratum: Phys. Rev.C95,no.4,049904(2017)], 1602.06580.
[10] F. Becattini, V. Chandra, L. Del Zanna, and E. Grossi, Annals Phys. **338**, 32 (2013), 1303.3431.
[11] R.-H. Fang, L.-G. Pang, Q. Wang, and X.-N. Wang, Phys. Rev. **C94**, 024904 (2016), 1604.04036.
[12] Q. Wang, Nucl. Phys. **A967**, 225 (2017), 1704.04022.
[13] L. Adamczyk et al. (STAR), Nature **548**, 62 (2017), 1701.06657.

- [14] J. Adam et al. (STAR), Phys. Rev. **C98**, 014910 (2018), 1805.04400.
- [15] M. Baznat, K. Gudima, A. Sorin, and O. Teryaev, Phys. Rev. **C88**, 061901 (2013), 1301.7003.
- [16] L. P. Csernai, V. K. Magas, and D. J. Wang, Phys. Rev. **C87**, 034906 (2013), 1302.5310.
- [17] L. P. Csernai, D. J. Wang, M. Bleicher, and H. Stoecker, Phys. Rev. **C90**, 021904 (2014).
- [18] O. Teryaev and R. Usubov, Phys. Rev. **C92**, 014906 (2015).
- [19] Yu. B. Ivanov and A. A. Soldatov, Phys. Rev. **C95**, 054915 (2017), 1701.01319.
- [20] H. Li, L.-G. Pang, Q. Wang, and X.-L. Xia, Phys. Rev. **C96**, 054908 (2017), 1704.01507.
- [21] D.-X. Wei, W.-T. Deng, and X.-G. Huang, Phys. Rev. **C99**, 014905 (2019), 1810.00151.
- [22] I. Karpenko and F. Becattini, Eur. Phys. J. **C77**, 213 (2017), 1610.04717.
- [23] Y. Xie, D. Wang, and L. P. Csernai, Phys. Rev. **C95**, 031901 (2017), 1703.03770.
- [24] Y. Sun and C. M. Ko, Phys. Rev. **C96**, 024906 (2017), 1706.09467.
- [25] J.-H. Gao, S.-W. Chen, W.-t. Deng, Z.-T. Liang, Q. Wang, and X.-N. Wang, Phys. Rev. **C77**, 044902 (2008), 0710.2943.
- [26] S. J. Brodsky, J. F. Gunion, and J. H. Kuhn, Phys. Rev. Lett. **39**, 1120 (1977).
- [27] T. Sjostrand, S. Ask, J. R. Christiansen, R. Corke, N. Desai, P. Ilten, S. Mrenna, S. Prestel, C. O. Rasmussen, and P. Z. Skands, Comput. Phys. Commun. **191**, 159 (2015), 1410.3012.
- [28] B. Andersson, G. Gustafson, and B. Nilsson-Almqvist, Nucl. Phys. **B281**, 289 (1987).
- [29] X.-N. Wang and M. Gyulassy, Phys. Rev. **D44**, 3501 (1991).
- [30] M. Gyulassy and X.-N. Wang, Comput. Phys. Commun. **83**, 307 (1994), nucl-th/9502021.
- [31] A. Adil and M. Gyulassy, Phys. Rev. **C72**, 034907 (2005), nucl-th/0505004.
- [32] K. A. Olive et al. (Particle Data Group), Chin. Phys. **C38**, 090001 (2014).
- [33] B. I. Abelev et al. (STAR), Phys. Rev. **C79**, 034909 (2009), 0808.2041.
- [34] L. Adamczyk et al. (STAR), Phys. Rev. **C96**, 044904 (2017), 1701.07065.
- [35] I. C. Arsene et al. (BRAHMS), Phys. Lett. **B687**, 36 (2010), 0911.2586.
- [36] I. G. Bearden et al. (BRAHMS), Phys. Rev. Lett. **94**, 162301 (2005), nucl-ex/0403050.
- [37] A. Andronic, P. Braun-Munzinger, K. Redlich, and J. Stachel, Nature **561**, 321 (2018), 1710.09425.
- [38] F. Becattini, J. Cleymans, and J. Strumpfer, PoS **CPOD07**, 012 (2007), 0709.2599.